Mon. Not. R. Astron. Soc. **371,** 1891–1897 (2006) doi:10.1111/j.1365-2966.2006.10844.x

Counting individual galaxies from deep 24-μm *Spitzer* surveys

G. Rodighiero,[1⋆] C. Lari,[2] F. Pozzi,[3,4] C. Gruppioni,[4] D. Fadda,[5] A. Franceschini,[1] C. Lonsdale,[6] J. Surace,[6] D. Shupe[6] and F. Fang[6]

[1]*Dipartimento di Astronomia, Università di Padova, Vicolo dell'Osservatorio 5, 351 22 Padova, Italy*
[2]*Istituto di Radioastronomia del CNR, via Gobetti 101, I-40129 Bologna, Italy*
[3]*Dipartimento di Astronomia, Università di Bologna, via Ranzani 1, I-40127 Bologna, Italy*
[4]*Istituto nazionale di Astrofisica, Osservatorio Astronomico di Bologna, via Ranzanis, I-40127 Bologna, Italy*
[5]*Spitzer Science Center, California Institute of Technology, MC 220-6, Pasadena, CA 91125, USA*
[6]*Infrared Processing and Analysis Center, California Institute of Technology, MC 100-22, Pasadena, CA 91125, USA*

Accepted 2006 July 17. Received 2006 July 17; in original form 2005 July 11

ABSTRACT

We address the question of how to deal with confusion-limited surveys in the mid-infrared (MIR) domain by using information from shorter-wavelength observations over the same sky regions. Such information, once applied to apparently extended MIR sources, which are indeed 'blends' of two or more different sources, allow us to disentangle the single counterparts and to split the measured flux density into different components. We present the application of this method to the 24-μm *Spitzer* archival data in the Great Observatories Origins Deep Survey ELAIS-N1 (GOODS EN1) test field, where apparently extended, 'blended' sources constitute about 20 per cent of a reliable sample of 983 sources detected above the 5σ threshold down to 40 μJy. As a shorter-wavelength data set, we have considered the public Infrared Array Camera (IRAC) images and catalogues of the same field. We show that the 24-μm sample is almost unbiased down to ∼40 μJy and the careful application of the deblending procedure does not require any statistical completeness correction (at least at the flux level considered). This is probed by direct comparison of our results with results in the literature that analysed the same data set through extensive Monte Carlo simulations. The extrapolation of the source counts down to fainter fluxes suggests that our 24-μm sample is able to resolve ∼62 per cent of the cosmic background down to a flux level of 38 μJy.

Key words: methods: data analysis – catalogues – galaxies: photometry – infrared: galaxies – infrared: general.

1 INTRODUCTION

Cosmological surveys in the mid-infrared (MIR)/far-infrared (FIR) spectral range reveal a substantial population of strongly evolving dust-enshrouded galaxies at intermediate redshifts (e.g. Elbaz et al. 1999; Franceschini et al. 2003). These galaxies are responsible for most of the cosmic infrared background (CIRB) detected at these wavelengths (Hauser & Dwek 2001). Although a significant fraction of the CIRB is already resolved into discrete sources by deep infrared surveys (i.e. ISOCAM has resolved about 60–70 per cent of the CIRB at 15 μm), to resolve the whole observed background light we should reach fainter flux limits.

However, the main limitation of deep surveys performed in the MIR/FIR domain is confusion due to extragalactic sources. In fact, the large number of distant galaxies in deep extragalactic surveys produces a high density of sources with respect to the instrument beam size. This makes more than one source responsible for the measured flux density at fainter limits, therefore producing incorrect source counts (i.e. higher than real at intermediate flux densities due to source 'blending') and limiting the effective survey sensitivity.

As recently suggested by Dole, Lagache & Puget (2006), we will show that it is possible to deal with this problem in deep extragalactic surveys by making use of shorter-wavelength observations in the same region of the sky. In particular, data obtained with the Infrared Array Camera (IRAC; Fazio et al. 2004) on board *Spitzer* in the 3.6- to 8.0-μm wavebands are extremely helpful for measuring fluxes of faint sources and reducing the confusion noise in surveys performed with the *Spitzer* Multiband Imaging Photometer (MIPS; Rieke et al. 2004) at 24, 70 or 160 μm. Through IRAC data, we have developed an efficient 'deblending' technique that allows us to accurately measure the flux density of sources detected by MIPS below the nominal confusion limit. The application of this technique to the Great Observatories Origins Deep Survey ELAIS-N1 (GOODS EN1) test field is presented in this paper.

⋆E-mail: rodighiero@pd.astro.it

The paper is structured as follows: in Section 2, we present the observations in the GOODS EN1 field; in Section 3, we describe the 24-μm data processing, we present the 24-μm catalogue and we discuss the 'deblending' technique; in Section 4, we show the number counts; and, in Section 5, we present our conclusions.

Throughout this paper, we will assume $H_0 = 75\,\mathrm{km\,s^{-1}\,Mpc^{-1}}$, $\Omega_\mathrm{m} = 0.3$ and $\Omega_\Lambda = 0.7$.

2 OBSERVATIONS

The EN1 field is one of the best areas, among those currently available, for investigating the effects of source confusion in MIR surveys. Deep MIPS 24-μm observations in this field cover an area of $\sim$185 arcmin^2 (centred at RA $16^\mathrm{h}09^\mathrm{m}20^\mathrm{s}$, Dec. $+54^\circ57'00''$) as part of the GOODS Science Verification programme of *Spitzer*. The field was observed in photometry mode. Two different Astronomical Observation Requests (AORs) were executed in cluster mode to observe the complete field. The integration time per detector pixel varies from $\sim$2000 s, in the lowest signal-to-noise ratio area, up to $\sim$4600 s in the highest signal-to-noise ratio regions. Details on the MIPS 24-μm data processing, source extraction and photometry will be given in the next section.

Although during the same verification observing campaign complementary deep observations of EN1 have been obtained with IRAC with the 3.6-, 4.5-, 5.8- and 8.0-μm channels, the combined IRAC GOODS maps do not perfectly overlap the whole MIPS GOODS image, thus leaving a fraction of the MIR map uncovered by IRAC data. However, a shallower and more extended observation of EN1 with the four IRAC channels has been performed as part of the *Spitzer* Wide-Area Infrared Extragalactic Survey (SWIRE) Legacy programme (Lonsdale et al. 2003), covering a much wider area (4 $\times$ 4 deg^2) and thus homogeneously overlapping the deeper GOODS verification MIPS data. Therefore, to have complete IRAC coverage of our MIPS image, we used the SWIRE map at 3.6 μm where GOODS data are not available.

Optical imaging of the GOODS EN1 field is provided by the First Look Survey (FLS) observations (Fadda et al. 2004). The *R*-band images were obtained using the Mosaic-1 camera on the 4-m Mayall Telescope of the Kitt Peak National Observatory. The images reach a median 5σ depth limiting magnitude of $R = 25.5$ (Vega) as measured within an aperture of 1.3 arcsec, for which the signal-to-noise ratio is maximal.

3 DATA PROCESSING

3.1 IRAC imaging

The reduction of GOODS data in the IRAC bands has been performed by starting from the basic calibrated data (BCD) obtained from the *Spitzer* archive. We subtracted the median background from each BCD frame. We then processed and mosaiced together all the corrected BCDs with the *Spitzer* MOPEX package[1] distributed by the Spitzer Science Center (SSC). We refer to Lonsdale et al. (2004) for a complete description of the observation strategy and data analysis of SWIRE.

The IRAC source extraction was performed with SExtractor (Bertin & Arnouts 1996), both on SWIRE and GOODS maps. For point-like sources, we computed the fluxes within a 6-arcsec-diameter aperture. We then applied a correction factor derived from the stars in the images to obtain the total fluxes in the IRAC bands. In the case of extended sources, we used Kron like magnitudes (AUTO_MAG output parameter in SExtractor). The IRAC photometry has been basically used to remove stars in the 24-μm catalogue.

[1] See http://ssc.spitzer.caltech.edu/postbcd

3.2 MIPS 24-μm imaging

We started the data analysis of the 24-μm data in the GOODS EN1 field from the archival BCD products. These have been preprocessed using version S10.0.3 of the SSC pipeline (see Spitzer Observer Manual). First, we have corrected each single BCD frame by computing a residual median flat-field, which depends on the scan mirror position. Such a flat-field has been built from the data.

By checking the temporal histories of each pixel, we observed a systematic drift of the signal (for details, see Fadda et al. 2006). We corrected this effect by applying a linear fit to the temporal sequence of each pixel. As a stabilization level, we choose the value of the final exposure frame. With this procedure, we produced background subtracted and flat-fielded frames that were co-added using the SSC software MOPEX to obtain a mosaic with half the original pixel scale (1.2 arcsec).

The projection algorithm applies a linear interpolation that accounts for the distortion corrections. Bad pixels are masked within the pipeline and cosmic rays are flagged using a multiframe temporal outlier detection. In Fig. 1, we show the signal-to-noise ratio map of the EN1 GOODS field observed by MIPS, which has been used for the source extraction (see Section 3.2.1).

In order to remove the Airy rings around sources, we have deconvolved the 24-μm image using the CLEAN task (typically used for analysing radio data), which is part of the National Radio Astronomy Observatories (NRAO) AIPS reduction package. The CLEAN algorithm iteratively finds and substracts positive features on the original map until the standard deviation of the residual image is lower than the noise level. The CLEAN map is then constructed by adding to the residual image the CLEAN components found, convolved with a Gaussian of the FWHM that is equal to that of the MIPS 24-μm point spread function (PSF; we computed a value of 5.5 arcsec by fitting the PSF provided with the used version of MOPEX). When the Gaussian beam and MIPS 24-μm PSF are normalized at the peak, the ratio between their total fluxes is 1:1.369. The mentioned procedure allows us to obtain a map (the CLEAN map) where the Airy rings are removed.

An example of the effects of applying the CLEAN procedure is illustrated in Fig. 2, where we report a zoom of 2.2 $\times$ 1.4 arcmin^2 into the map presented in Fig. 1. The left panel shows the original flux map and the right panel shows the corresponding CLEANed map, which shows that the adopted approach is efficient in deconvolving many close sources, providing a reconstructed map where the confusion due to first Airy ring is reduced.

3.2.1 Source extraction

Before performing source extraction, we have applied a recursive median filtering to the final mosaic map. The size of the box used to computed the median is 64 $\times$ 64 pixels of 1.2 arcsec. This procedure is used in order to smooth residual spurious background fluctuations. Source detection is then performed on the signal-to-noise ratio map by selecting all pixels above a low flux threshold (0.5 μJy pixel^{-1}) using the IDL Astronomy Users Library routine called FIND (based on the equivalent algorithm of DAOPHOT). We then extract from the detection list only those objects with a value of the signal-to-noise ratio of the peak pixel greater than 5. The preliminary list includes 953 sources. The combination of long

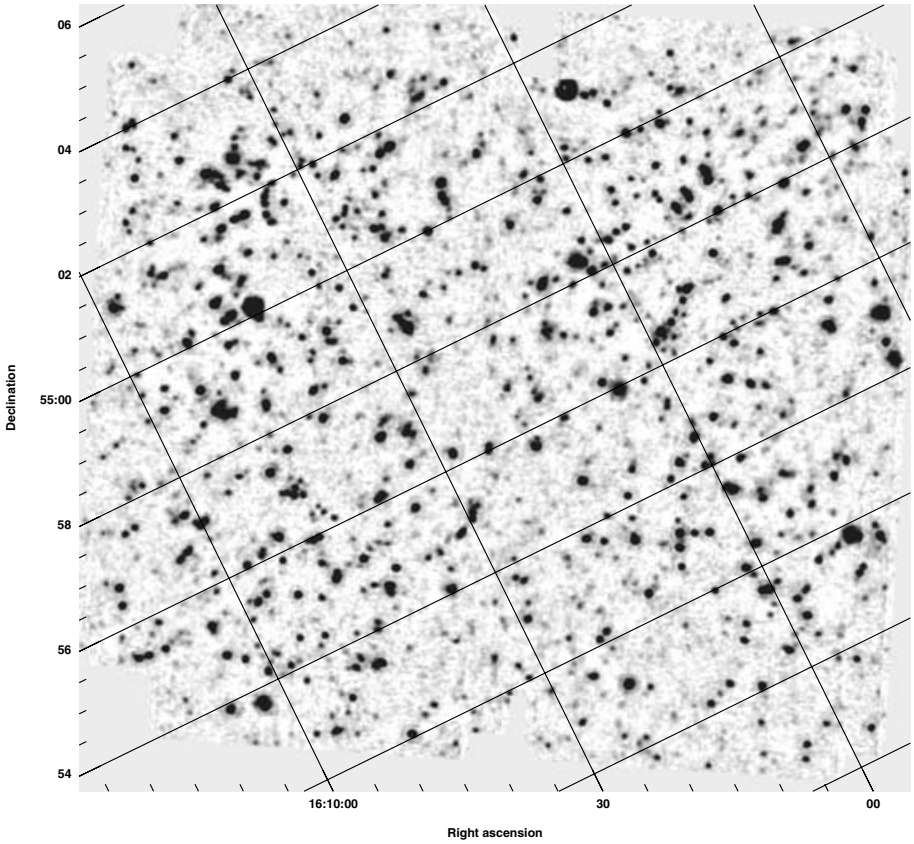

Figure 1. Signal-to-noise ratio map of the deep EN1 field observed by MIPS.

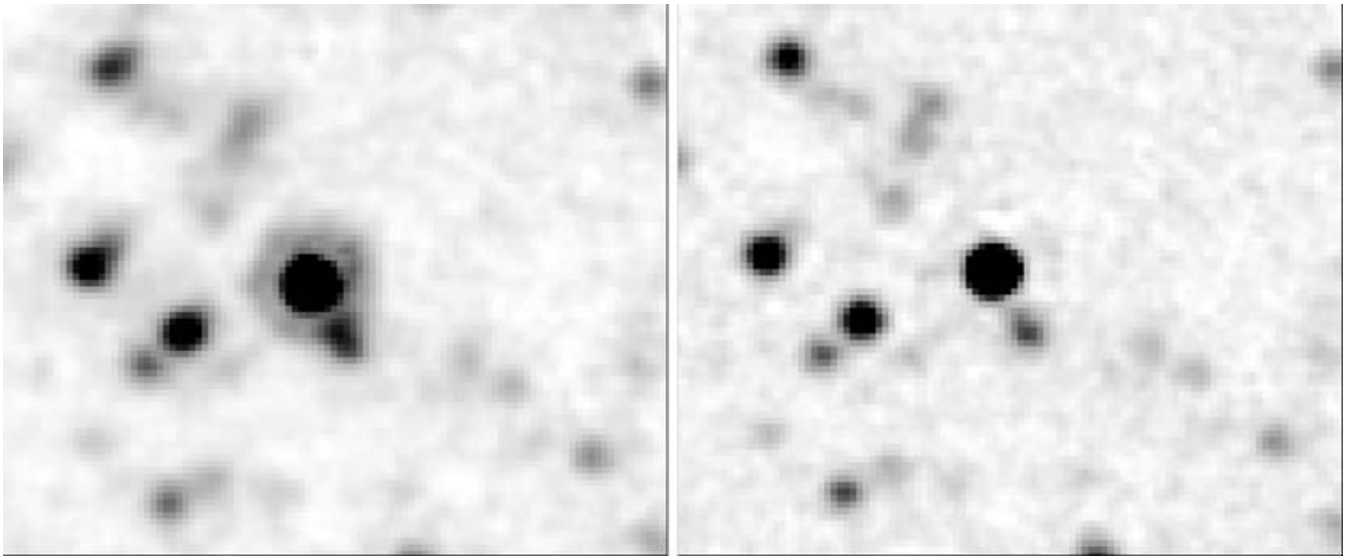

Figure 2. Example of the effects of applying the CLEAN task to the flux map. We report a zoom of 2.2×1.4 arcmin^2 into the map presented in Fig. 1. The left panel shows the original flux map and the right panel shows the corresponding CLEANed map, which shows that the adopted approach is efficient in deconvolving many close sources, providing a reconstructed map where the confusion due to first Airy ring is reduced.

exposure times and high repetition factor of this *Spitzer* survey provides a very deep infrared observation of the sky that is basically confusion-limited. For this reason, we checked each detected source by visual inspection. We exploited the availability of shorter-wavelength observations from IRAC (see Section 2) to look for the counterparts of eventual blended MIPS sources. Indeed, the better resolution of the *Spitzer* near-infrared (NIR) data allows one to disentangle the multiple components of the MIR sources. We found that 21 per cent of 953 sources are 'blended'. These objects have generally pairs or small groups as IRAC/optical counterparts. A representative sample of this class is shown in Fig. 3, where for each blend case we report both infrared (IRAC 3.6, left panel) and

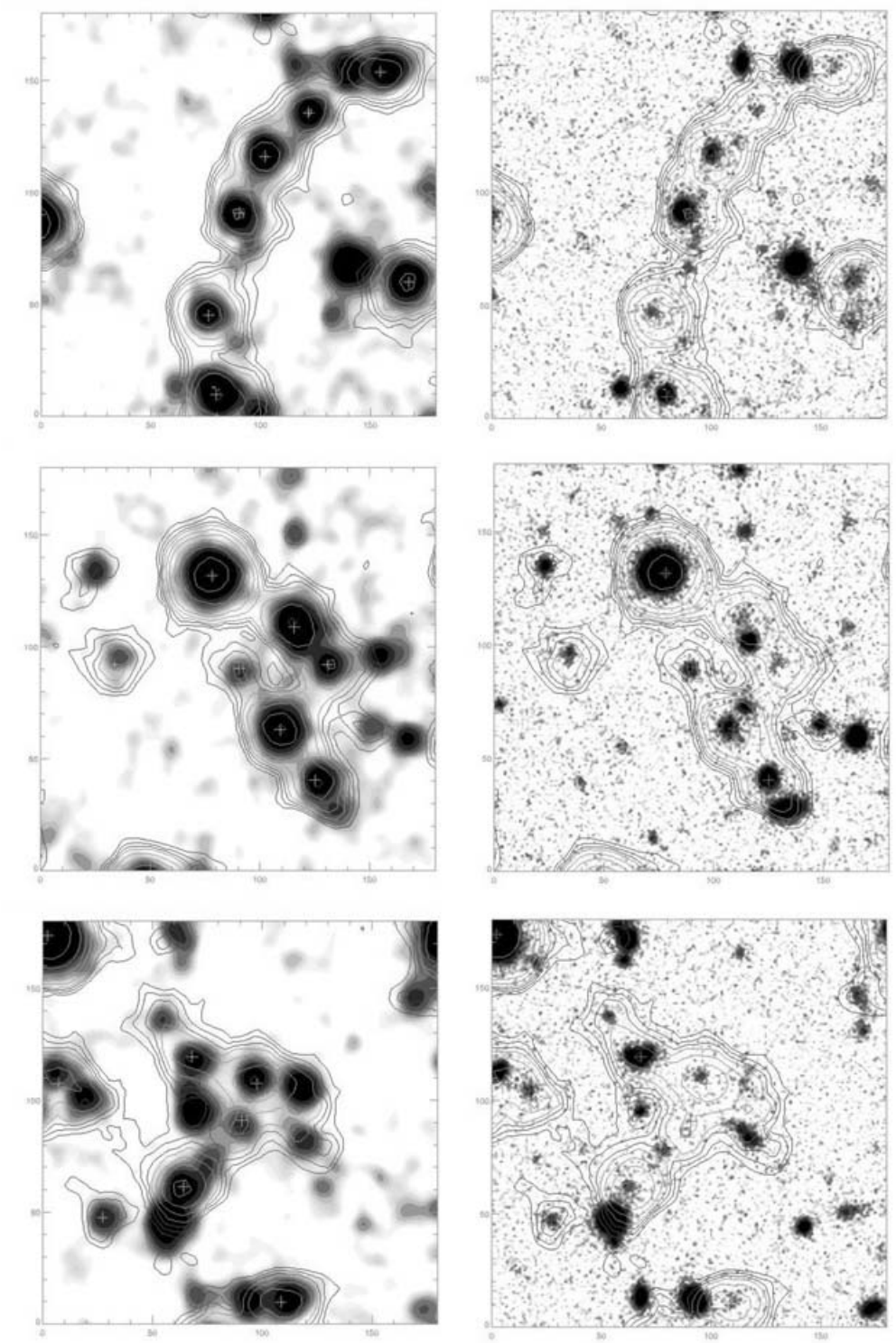

Figure 3. Example of three blend 24-μm sources. For each case, we report both the NIR (IRAC 3.6 μm, left panel) and the optical (*R* band, right panel) images overlayed with the MIPS 24-μm contours, starting from the 2σ level at increasing values. North is up and east at left. Each image is 50×50 arcsec^2. The crosses mark the positions of the 24-μm sources in the catalogue with a signal-to-noise ratio of greater than 5.

optical (*R* band, right panel) images overlayed with the MIPS 24-μm contours ($>3\sigma$).

3.2.2 MIPS 24-μm photometry

In order to obtain an optimized photometry at each flux level, we used the following approaches.

(i) For the few extended sources (three), aperture photometry was computed.

(ii) In the case of bright (S/N $> 7\sigma$, value computed in correspondence of the peak pixel) and isolated point-like sources, we applied a PSF-fitting algorithm (IMFIT, within the AIPS environment) to perform photometry.

Table 1. First 10 entries of the 24-μm source catalogue in the EN1 test field.

ID	RA (^{h} ^{m} ^{s})	Dec. ($^\circ$ $'$ $''$)	S/N	S(24 μm) (μJy)
EN1-160855+550112	16 08 55.87	55 01 12.05	194	3169
EN1-160942+550009	16 09 42.66	55 00 09.48	191	1692
EN1-160906+545557	16 09 06.53	54 55 57.38	94	791
EN1-160904+545821	16 09 04.47	54 58 21.75	94	1131
EN1-160848+545150	16 08 48.87	54 51 50.46	92	1265
EN1-160936+550242	16 09 36.91	55 02 42.39	69	590
EN1-160921+545109	16 09 21.50	54 51 09.93	62	741
EN1-160839+545523	16 08 39.85	54 55 23.39	62	586
EN1-161003+545344	16 10 03.27	54 53 44.77	57	851
EN1-160839+545523	16 08 39.85	54 55 23.39	54	586

(iii) A different approach is required in the case of confused and blended sources. We have examined each single MIPS blend source and determined the multicounterparts looking at the IRAC image. When the associations are not clear, we refer to the optical *R*-band frames that allow us to visually check and solve most of the ambiguous cases. Once the number and the positions of the counterparts of a MIR blend source are fixed, then same PSF-fitting algorithm mentioned above was applied to compute an accurate photometric deblending on the CLEAN map. Blended sources are assumed to be point-like sources. This provides a measure of the 24-μm flux of each confused component.

(iv) For the faintest and isolated point-like sources in our catalogue (S/N $< 7\sigma$, again the value is computed in correspondence of the peak pixel), the 24-μm flux density was computed by applying a correction factor to the measured peak flux, in order to convert the peak flux into a total flux density. The correction factor is basically computed from the *Spitzer* MIPS PSF, provided within the MOPEX package (as of 2006 January), and is found to have a value of 34.35. This method has been already extensively applied and validated by us when dealing with ISOCAM 15-μm data (Lari et al. 2001; Fadda et al. 2004; Rodighiero et al. 2004; Vaccari et al. 2005). In this work, the standard calibration from the SSC is applied. Future detailed measures of stellar fluxes, to be compared with atmosphere model predictions, will provide a more robust absolute calibration for *Spitzer* photometry. The MIPS 24-μm absolute flux calibration is correct within a few per cent. We have already shown the good correlation between peak and aperture fluxes in the case of the shallow MIR survey (Vaccari et al. 2005, fig. 15).

Our algorithm for the computation of peak fluxes is optimized to account for the coarse sampling of the 24-μm map, applying a suited resampling of the image before performing the photometry. In this way, we can account for the fact that the peak value of a source would change significantly depending on whether the true peak falls on a pixel centre or between pixels (for details on the algorithm see Lari et al. 2001).

At the end of this analysis, the final MIPS sample in the GOODS EN1 field includes 983 sources detected above the 5 σ threshold.

3.2.3 *The 24-μm GOODS EN1 catalogue*

In Table 1, we report a tabulation of the first 10 rows of the final catalogue of 24-μm detections in the GOODS EN1 validation field. The complete catalogue[2] contains 983 sources detected above 5σ.

[2] The complete catalogue in ASCII format is made publicly available through the World Wide Web at http://dipastro.pd.astro.it/giulia/EN1/ver or directly from the authors on request.

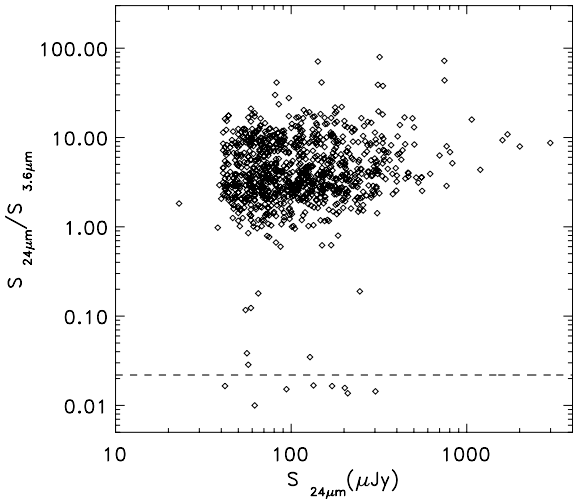

Figure 4. S(24 μm)/S(3.6 μm) flux ratio as a function of the 24-μm flux for the sources in the final catalogue. The dashed horizontal line marks the Rayleigh–Jeans ratio. We classified as stars all sources with S(24 μm)/S(3.6 μm) < 0.1.

The faintest source corresponds to a flux level of 24 μJy. The five entries in the table are: the International Astronomical Union (IAU) source designation, right ascension and declination (J2000), signal-to-noise ratio, and total 24-μm flux density (in μJy). Fluxes marked on the right side with an asterisk indicate the 11 sources classified as stars. Fig. 4 shows the distribution of the S(24 μm)/S(3.6 μm) flux ratio as a function of the 24-μm flux for the sources in the final catalogue. This NIR to MIR colour is an efficient star/galaxy separator (a similar technique was already used by us for 15-μm ISOCAM sources, Rodighiero et al. 2004). The dashed horizontal line marks the Rayleigh–Jeans ratio. We classified as stars all sources with S(24 μm)/S(3.6 μm) < 0.1. The few points above the dashed line correspond to elliptical galaxies.

The flux uncertainties are basically given by the signal-to-noise ratio.

3.2.4 *Effects of confusion*

To quantitatively estimate the global effect of confusion in the EN1 GOODS 24-μm map, we have measured the density of galaxy pairs at increasing distance scale. The result is shown in Fig. 5.

For each single source, we have counted the number of detections falling within a circle of radius r centred on the source position. This is recursively done for different increasing values of r and for all the sources in the catalogue. The median value of the source density at each distance r is normalized to a circular area with radius of 5.5 arcsec and plotted against r. The solid line in the figure is computed using the preliminary 5σ catalogue before deblending the confused sources (it includes 953 sources), while the dashed line has been built from the final deblended catalogue (983 sources). No corrections were applied for the variable noise, but only for the geometry as the larger circles are limited by the boundary of the map. This analysis indicates the completeness of our method: the only sources that we are not able to deblend are those too close to each other (angular separation lower than ∼6 arcsec). Obviously, identifications from higher-resolution instruments may help, but if the separation is too small, even IRAC observations might suffer confusion problems. A Monte Carlo simulation test can recover

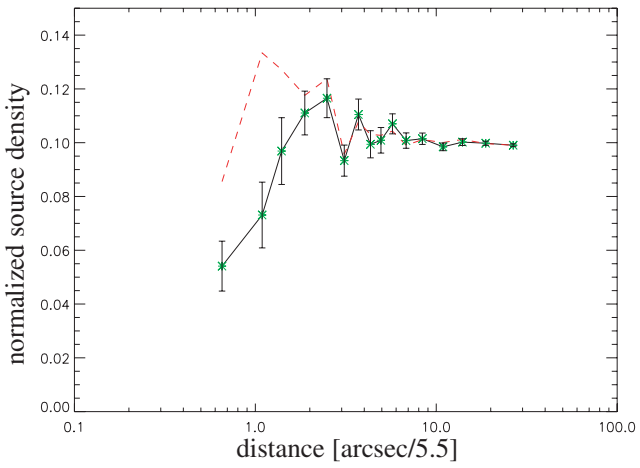

Figure 5. Number of detections falling within a circle of radius r (centred on the source position) normalized to a circular area with radius of 5.5 arcsec, as a function of distance r for all the sources in the catalogue. The solid line represents the preliminary 5σ catalogue before deblending the confused sources. The dashed line represents the final deblended catalogue.

these small deficits when dealing with source counts, however we have been very conservative when computing the source counts, cutting at a flux level that is not affected by the mentioned problem.

4 EXTRAGALACTIC NUMBER COUNTS

To study the statistical properties of our sample and to alternatively check the effects of confusion on our results, we have computed the extragalactic source number counts. Stars were removed from this compilation. We have computed the 24-μm source counts down to a flux level of ∼30 μJy. The counts have been obtained by weighting each single source for the effective area corresponding to its flux density.

In Fig. 6, we report the differential 24-μm counts normalized to the Euclidean law ($\mathrm{d}N/\mathrm{d}S \propto S^{-2.5}$). We compare the distribution

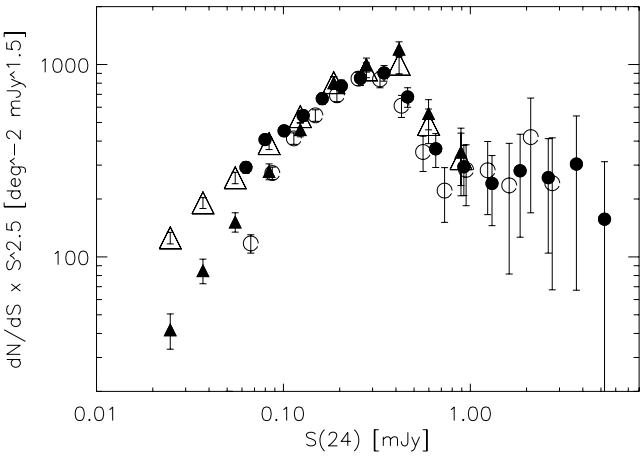

Figure 6. Differential 24-μm counts normalized to the Euclidean law ($N \propto S^{-2.5}$). We compare the distribution obtained by using our final deblended catalogue (filled circles, 983 sources) and the preliminary 5σ catalogue prior to deblending (open circles, 953 sources). We compare our results with the source counts by Chary et al. (2004). The filled triangles refer to their uncorrected counts and the open triangles correspond to their final completeness corrected data.

obtained by using our final deblended catalogue (filled circles, 983 sources) and the preliminary 5σ catalogue obtained before deblending (open circles, 953 sources). The differential source counts have been obtained by weighting each single source for its effective area, rather than weighting the total number of sources in each flux density bin for the effective area corresponding to the reference flux density of the bin. The errors associated with the counts in each bin have been computed as $\sqrt{\sum_i 1/A_{\mathrm{eff}}^2(S_i)}$, where the sum is for all the sources with flux density S_i and $A_{\mathrm{eff}}(S_i)$ is the effective area corresponding to that flux. The quoted errors have to be considered as lower limits of the total errors.

The two distributions reported in Fig. 6 clearly show that, when accounting for confusion, the density of faint sources is generally increased, and the source counts slope is less steep (by a factor of ∼2) below the peak observed at ∼0.2 mJy.

In Section 3.2.4, we argued that an accurate deblending analysis might provide unbiased complete samples. This is quantitatively confirmed if we compare our results with those derived by Chary et al. (2004). Chary et al. (2004) started from the same data set in the EN1 GOODS 24-μm field, but they did not treat each single source by looking at the counterparts in the IRAC map. They followed a statistical approach to studying the properties of the 24-μm population. Their completeness corrections were measured using a Monte Carlo approach: by adding artificial sources on the original mosaic, they were able to recover the fraction of undetected/lost sources as a function of the flux level combined with their extraction procedure. In Fig. 6, we report also the source counts by Chary et al. (2004) for comparison with our estimate. The filled triangles refer to their uncorrected counts, while the open ones correspond to their final completeness corrected data.

The comparison between the Chary et al. (2004) counts and ours shows a remarkable consistency (see Fig. 6). This result is a direct demonstration that we do not need to apply any statistical correction to our sample, which turns out to be almost unbiased down to relatively faint fluxes (40 μJy).

Dole et al. (2004) have computed the confusion limit for each MIPS *Spitzer* band. They report three different estimates based on different methods: 56 μJy (from the source density criterion; Dole, Lagache & Puget 2003), 71 and 141 μJy (levels deduced from the source density of one source per 20 and 40 independent beams). Dole et al. (2003) have also estimated that the use of a Gaussian PSF (as in the case of the CLEANed image) instead of a simulated *Spitzer* PSF changes the confusion limit by only 2 per cent in the 24-μm MIPS band. This implies that, in a MIPS image, the choice of a Gaussian PSF versus a realistic *Spitzer* PSF does not change the confusion limit very much (a few per cent at most) as long as the FWHMs of these PSFs are the same. With the photometric procedure adopted in this work, we are able to detect a complete sample of 24-μm sources below the nominal confusion limit (even considering the lowest value reported by Dole et al. 2004).

In Fig. 7, in addition to comparing our source counts (filled circles) to those of Chary et al. (2004, open triangles), we show also those from Papovich, Dole & Egami (2004, filled triangles). We also report the 24-μm counts published by Marleau et al. (2004, open circles).

Although Fig. 7 shows a general agreement between the analyses of the flux (at low fluxes: 0.03–0.3 mJy) of four independent 24-μm counts over about a decade, at fluxes brighter than 0.3 mJy the GOODS N1 statistic is quite poor as the field was explicitly chosen to avoid bright MIR sources (based on the positions of ISOCAM sources). The study of Papovich et al. (2004) is based on a much wider area (∼10 deg^2), split into different sky regions. Poor statistics

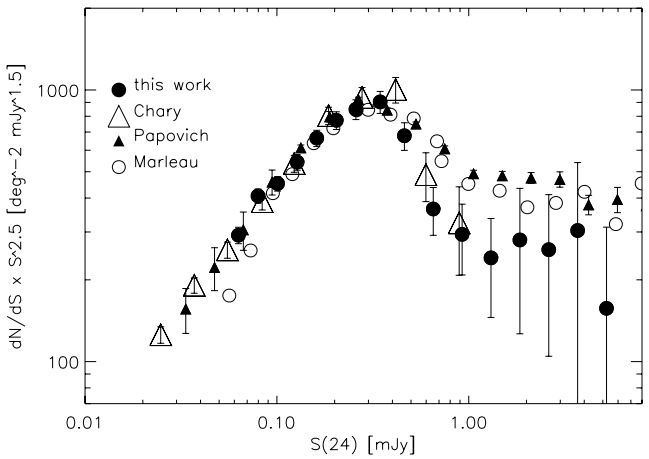

Figure 7. Differential 24-μm counts normalized to the Euclidean law. We compare our source counts (filled circles) with those of Chary et al. (2004, open triangles), Papovich et al. (2004, filled triangles) and Marleau et al. (2004, open circles).

and cosmic variance on small scales (as the size of the EN1 field) can be the reason for the counts discrepancy observed above 0.3 mJy.

By integrating our source counts down to $S(24\,\mu\mathrm{m}) = 38\,\mu$Jy, we have obtained an estimate of the 24-μm cosmic background intensity down to that flux level: $1.63\,\mathrm{nW\,m^{-2}\,sr^{-1}}$. We have then extrapolated the differential source counts, fitting the fainter flux bins with a power law (slope $= -0.58$) to obtain an estimate of the expected value of the total background at 24 μm: $2.6\,\mathrm{nW\,m^{-2}\,sr^{-1}}$. The fraction of the background that we resolve down to 38 μJy is about 62 per cent. This value is also in agreement with the extrapolation of Chary et al. (2004) based on the same data set (they conclude that these deep *Spitzer* observations have resolved out at least 50 per cent of the 24-μm extragalactic background light and probably as much as 65 per cent).

Papovich et al. (2004) report a value for the total background intensity at 24 μm of $2.7\,\mathrm{nW\,m^{-2}\,sr^{-1}}$, quite in agreement with our estimate. However, they are able to resolve up to 70 per cent of the background already at 60 μJy. This difference is probably related to the extrapolation mode applied at the faint end of the source counts.

5 SUMMARY

We have analysed a deep MIPS 24-μm survey in the EN1 region, conceived as a validation observation for the official GOODS strategy (Dickinson 2004). The archival *Spitzer* data of the GOODS EN1 test field allowed us to check the effects of source confusion on the MIR statistics. We have processed the data to obtain a final mosaic that is basically confusion-limited. To deal with confusion, we have applied the CLEAN algorithm to the 24-μm map, removing the diffraction rings around bright sources. Few blend sources are then partially recovered and appear as resolved objects in the CLEANed map. A different approach is needed for confused sources with closer single counterparts. We used the information from shorter-wavelength observations in the same regions in order to detect the counterparts of the apparently extended 24-μm blend sources. An optimal solution is provided by the NIR camera on board *Spitzer*, IRAC. In particular, we have referred to the 3.6- and 4.5-μm maps to associate the single counterparts to the subcomponents of the 24-μm unresolved emission. An optical *R*-band image (Fadda et al. 2004) has also been considered for disentangling a few dubious cases. We have then obtained a reliable 24-μm catalogue including 983 sources at the 5σ level, the fainter source reaching a flux of 24 μJy. We have shown that our sample is almost unbiased down to ∼40 μJy and that, by applying a deblending procedure, we do not need to apply any statistical completeness correction (at least to the flux level considered). This is probed by direct comparison of our results with those of Chary et al. (2004), who analysed the same data set through extensive Monte Carlo simulations.

We have compared the 24-μm extragalactic source counts derived from our sample with those published by Chary et al. (2004) and Papovich et al. (2004). We found a good agreement between the different data sets, when reporting the counts of the other authors to the same flux scale. At the bright end, the GOODS EN1 test field is biased by low statistics and probably cosmic variance, resulting in an underdensity of bright sources at >0.3 mJy with respect to larger area surveys (Papovich et al. 2004).

By extrapolating the source counts to fainter fluxes, we have estimated the fraction of the cosmic background already resolved by our sample down to a flux level of 38 μJy: ∼62 per cent.

ACKNOWLEDGMENTS

We thank an anonymous referee for careful comments that improved the quality of the paper. This work is based on observations made with the *Spitzer Space Telescope*, which is operated by the Jet Propulsion Laboratory, California Institute of Technology under NASA contract 1407.

REFERENCES

Bertin E., Arnouts S., 1996, A&AS, 117, 393
Chary R. et al., 2004, ApJS, 154, 80
Dickinson M., 2004, A&AS, 205, 1614
Dole H., Lagache G., Puget J.-L., 2003, ApJ, 585, 617
Dole H. et al., 2004, ApJS, 154, 93
Dole H., Lagache L., Puget J. L., 2006, in Armus L., ed., ASP Conf. Ser. Vol., The Spitzer Space Telescope: New Views of the Cosmos. Astron. Soc. Pac., San Francisco, in press (astro-ph/0503017)
Elbaz D. et al., 1999, A&A, 351, L37
Fadda D., Jannuzi B. T., Ford A., Storrie-Lombardi L. J., 2004, AJ, 128, 1
Fadda D. et al., 2006, AJ, 131, 2859
Fazio G. G. et al., 2004, ApJS, 154, 10
Franceschini A. et al., 2003, A&A, 403, 501
Hauser M. G., Dwek E., 2001, ARA&A, 39, 249
Lari C. et al., 2001, MNRAS, 325, 1173
Lonsdale C. J. et al., 2003, PASP, 115, 897
Lonsdale C. J. et al., 2004, ApJS, 154, 54
Marleau F. R. et al., 2004, ApJS, 154, 66
Papovich C., Dole H., Egami E., 2004, ApJS, 154, 70
Rieke G. H. et al., 2004, ApJS, 154, 25
Rodighiero G., Lari C., Fadda D., Franceschini A., Elbaz D., Cesarsky C., 2004, A&A, 427, 773
Vaccari M. et al., 2005, MNRAS, 358, 397

This paper has been typeset from a TEX/LATEX file prepared by the author.